CHALMERS
UNIVERSITY OF TECHNOLOGY

Characterisation of Droplet Formation in Spray Drying of Inhaled Medicines

Master's thesis in Innovative and Sustainable Chemical Engineering

ROHIT PAWSE

DEPARTMENT OF CHEMISTRY AND CHEMICAL ENGINEERING

CHALMERS UNIVERSITY OF TECHNOLOGY

Gothenburg, Sweden 2022

www.chalmers.se

Characterisation of Droplet Formation in Spray Drying of Inhaled Medicines

ROHIT PAWSE

Master's thesis 2022
Department of Chemistry and Chemical Engineering
Chalmers University of Technology
SE-412 96 Gothenburg
Telephone +46 (0)31-772 1000

Inhalation Product Development, Pharmaceutical Technology & Development, AstraZeneca, Gothenburg, Sweden

Supervisor: Katrin Walter, Formulation, Inhalation Product Development, Pharmaceutical Technology & Development, AstraZeneca, Gothenburg, Sweden

Supervisor: Karin Sundström, Formulation, Inhalation Product Development, Pharmaceutical Technology & Development, AstraZeneca, Gothenburg, Sweden

Supervisor: Ingela Niklasson Björn, Process Engineering, Inhalation Product Development, Pharmaceutical Technology & Development, AstraZeneca, Gothenburg, Sweden

Supervisor: Duy Nguyen, Process Engineering, Inhalation Product Development, Pharmaceutical Technology & Development, AstraZeneca, Gothenburg, Sweden

Examiner: Ronnie Andersson, Professor, Chemistry and Chemical Engineering, Chalmers University of Technology, Gothenburg, Sweden

Cover: Close-up of a spray formed by a Schlick 970 S4 nozzle imaged at 30,000 fps.

Gothenburg, Sweden 2022

Characterisation of Droplet Formation in Spray Drying of Inhaled Medicines

ROHIT PAWSE
Department of Chemistry and Chemical Engineering
Chalmers University of Technology

Abstract

Spray-drying is an established method for manufacturing of inhaled medicines. It facilitates the engineering of particles and control over various attributes of particle formation. An important step in this process is spraying, which is used to atomise the solvent solution into fine droplets. These atomised droplets are then dried in the presence of hot air to form particles. Spray dried particles have specific requirements when it comes to solid particle size and therefore control over particle size is one of the key factors necessary to the success of this technology. Spray formation and atomisation are however not well understood phenomenon and strong links between droplet formation and particle formation are found in theory. Hence, a good understanding of how droplet formation occurs and can be controlled is essential for the successful engineering of spray-dried particles. In this thesis, a Schlick 970 S4 nozzle was used to study the influence of composition on droplet size using formulations with different compositions of surface-active excipients and Active Pharmaceutical Ingredients (API). A Malvern Spraytec was used to determine the droplet size distribution at a selected range of flow parameters and changes in atomisation characteristics were studied by comparing the changes in droplet sizes for various formulations at the same flow parameters. The influence and effect of process parameters mainly liquid and gas flowrates on droplet formation are also studied and trends are plotted. It is found that gas flowrate is the primary parameter affecting the droplet formation and limitations on using the gas flowrate to manipulate the droplet size are identified. The main findings of this work indicate that the presence of surface-active excipients and API result in a reduction of droplet size and in turn solid particle size. This finding is further strengthened by correlating droplet size data with solid particle size data resulting in a good correlation for Dv50 and Dv90 values. Change in compositions ultimately result in changes to the physical properties of the solution namely, surface tension and viscosity. It is then explored how changes in surface tension and viscosity lead to changes in droplet size and strong correlations are observed. These strong correlations are then justified through mechanisms in theory and the cause effect relationship is identified. An attempt is also made using a high-speed camera to identify breakup mechanisms for use in future studies.

Keywords: Atomization, Nozzles, Spray-Drying, Droplet Size Measurements

Acknowledgements

I would like to sincerely thank Katrin Walter for giving me the opportunity of working on this Master Thesis at AstraZeneca. I feel grateful for having your endless guidance and tireless support for this project. I would also like to thank Karin Sundström, Ingela Niklasson Björn, Duy Nguyen & Ronnie Andersson for their constant guidance in this project. You all helped pave the way for this project and take it a step further. I extend my gratitude to Magnus Svensson for all the help with the formulations and company throughout this project. Lastly, I would also like to thank everyone who contributed to this project in every small way.

This project has been funded by **AstraZeneca.**

Rohit Pawse, Gothenburg, August 2022

Table of Contents

Nomenclature

Latin symbols

d_0	Primary droplet diameter	[m]
d_l	Orifice diameter	[m]
Dv10	Diameter at which 10% of the total volume of spray is made up of droplets with equal or lower diameters	[m]
Dv50	Diameter at which 50% of the total volume of spray is made up of droplets with equal or lower diameters	[m]
Dv90	Diameter at which 90% of the total volume of spray is made up of droplets with equal or lower diameters	[m]
l	Characteristic length	[-]
M	Momentum ratio	[-]
M_c	Critical momentum ratio	[-]
Oh	Ohnesorge number	[-]
Re_l	Reynolds number liquid	[-]
U_l	Velocity of liquid	[m/s]
U_g	Velocity of gas	[m/s]
v	Velocity	[m/s]
We	Weber number	[-]

Greek symbols

μ	Viscosity	[Kg/m-s]
μ_d	Viscosity of droplet	[Kg/m-s]
ρ	Density	[Kg/m^3]
ρ_g	Density of gas	[Kg/m^3]
ρ_d	Density of droplet	[Kg/m^3]
ρ_l	Density of liquid	[Kg/m^3]
σ	Surface tension	[N/m]

Abbreviations

ALR	Air to Liquid Ratio
API	Active Pharmaceutical Ingredient
CFD	Computational Fluid Dynamics
GFQ	Gas Flowrate
KH	Kelvin-Helmholtz
LFQ	Liquid Flowrate
M-NS	Modified Navier-Stokes
NS	Navier-Stokes
PSD	Particle Size Distribution
RT	Rayleigh-Taylor
SD	Standard Deviation
SE	Standard Error
TAB	Taylor Analogy Breakup

1. Introduction

Spray drying is considered an effective manufacturing technique for particle engineering and is widely used in the food and pharmaceutical industry. Various attributes of the final particles can be engineered via the spray drying process. It is an effective process for manufacturing of fine particles required to address dissolution rate (e.g., milk powder or instant coffee), bioavailability for poorly soluble APIs (Pharmaceutical Active Substance) or stability (for inhaled biologics). Inhalable medicines have specific requirements when it comes to particle size and these can be catered to through the spray drying process. In order to reach the lung and be effectively absorbed these particles need to be in a certain particle size range. Particles above 5µm cannot enter the lungs and are usually deposited in the upper airways, whereas particles below 1µm recirculate with breaths and are exhaled out of the respiratory system. This is where spray drying becomes a key manufacturing process owing to its particle engineering capabilities. Spray drying consists of 3 major process steps namely, formation of the droplets through atomisation of feedstock, drying of droplets to form solid particles and separation of these particles according to desired particle size. A schematic representation of the spray drying process is shown in Figure 1.

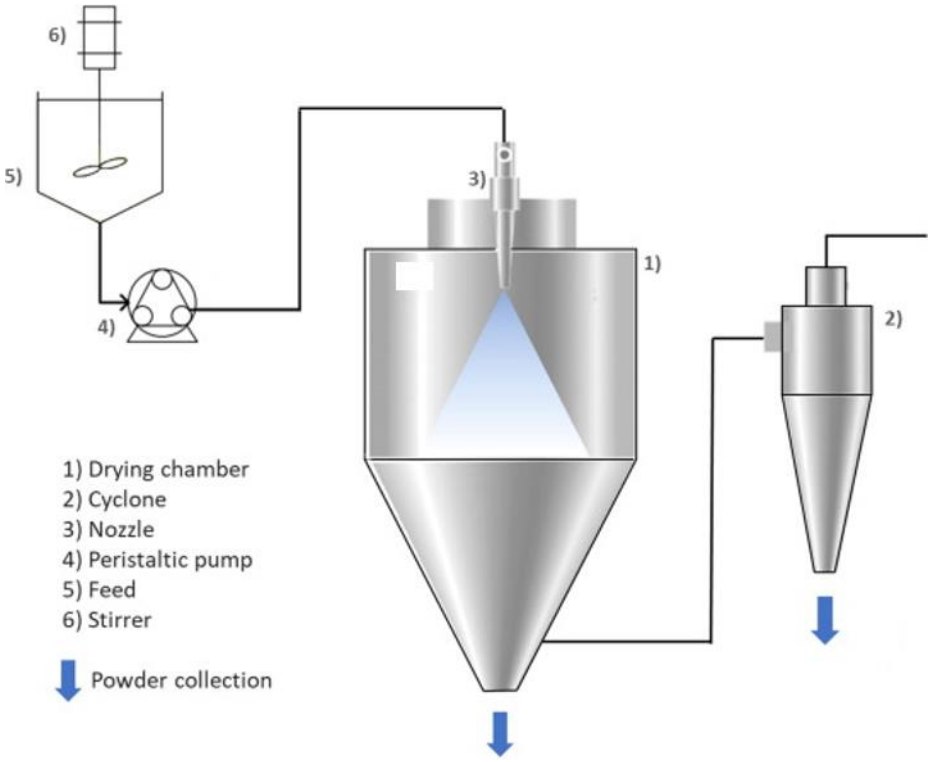

Figure 1: Schematic of spray drying process (Gil-Chávez, Padhi, Hartge, Heinrich, & Smirnova, 2020) .

In the first step of the spray drying process, the feedstock solution is pumped to a nozzle which atomises the solution liquid into fine droplets. In the next step, these atomised droplets come in contact with hot air in the drying chamber where the solvent is evaporated from the droplet to form a solid particle. In the last step, a cyclone separator is used to strip the drying gas of solid particles. Understanding the spray drying process and control of the process parameters are critical to ensure the right attributes of the solid particulate material. It ensues that each of these stages is controlled by various physical mechanisms and therefore an extensive study of how alterations to composition of formulations, process parameters, physical properties, and design characteristics of the nozzle, drying chamber and cyclone lead to changes in solid particles is required for effectively controlling the

particle size. Thus, understanding the spray drying process and control of the process parameters are critical to ensure the right attributes of the solid particulate material.

It was of interest to study the impact of change in composition of excipients on change in solid particle size. The presence of a surface-active excipient was suspected as the primary facilitator for change in particle size. In literature a strong evidence of relation between the droplet and the particle size can be found. Works of (Alhajj, O'Reilly, & Cathcart, 2021); (Reinhard, 2008); (Boel, et al., 2020) offered evidence that these changes in particle size had already developed at the droplet stage of the particles. A hypothesis was then made that a change in the composition of excipients resulted in a change in solid particle size and that this change in size could be observed at the droplet stage of particle formation. Therefore, an investigation was to be made to test if changes in size could be found in the early stages of the spray drying process i.e., atomisation. Further, it is of interest to understand what leads to these differences in droplet sizes. Therefore, the primary focus of this thesis is to investigate the atomisation and its effects on droplet size.

Atomisation

Atomisation is the process of turning bulk liquid into tiny droplets. Atomisation is broadly classified as hydraulic atomisation and pneumatic atomisation. In hydraulic atomisation, the liquid is forced through an orifice using high pressure. This pressure is then converted to velocity and results in the formation of droplets due to breakup. In pneumatic atomisation, air is used to create turbulence in a stream and result in atomisation. A spray nozzle is the device used to achieve atomisation.

Spray nozzle

A spray nozzle is the heart of the atomisation process. Spray nozzles can be classified based on various characteristics that they offer. They can be classified based on their functions, pattern, mechanism, etc. The nozzle used in this thesis is a pneumatic type of nozzle manufactured by Dusen-Schlick. The model of nozzle is Schlick 970 S4. Schlick 970 S4 is an external mixing, full cone, pneumatic atomising type of nozzle. It consists of two inlets, one for liquid and one for atomising air. External mixing refers to the phenomenon that the liquid and air come in contact with each other after they exit the nozzle. Conversely, in an internal mixing nozzle, the liquid and air mix inside the nozzle and are ejected from the orifice of the nozzle. A full cone refers to shape of the plume developed by the nozzle. The spray resembles the shape of a cone. The construction of the nozzle is shown in Figure 2 below.

Figure 2: Construction of the Schlick 970 nozzle used (Dusen-Schlick GmBH, 2022).

The nozzle can be customised based on various requirements. Different diameters of the liquid orifice are available as well as the length of the body can be adapted/adjust to match that of the requirements of the equipment. The tip of the liquid orifice insert can be extended to prevent clogging of the nozzle under high air pressure. An important aspect of the nozzle is that it is a swirling flow type of atomisation nozzle. Spray drying equipment primarily used the 0.8mm type of nozzle as the atomiser. It was also of interest to understand the differences in the different liquid orifice diameters and therefore of the available options of 0.3, 0.5 and 0.8, it was chosen to only study the 0.5mm nozzle to decrease the complexity of the study. Based on the specification by Schlick it is assumed that the primary difference they offer is in the capacity of liquid flow that can be delivered using these different

orifice sizes. Schlick also offers different spacer rings that determine the air cap position. The air cap position helps manipulate the air flowrate through the nozzle. The default air cap position is used for all the experiments.

Understanding the nozzle with respect to spray drying

The choice of nozzle recommended is discussed based on various factors given below. These are based on overall reflections and understanding of the author.

Pneumatic atomisation

In pneumatic atomisation, the driving force for atomisation is supplied by air. On the contrary, in hydraulic atomisation the driving force for atomisation is supplied by pressure exerted on the liquid. Since the nozzle is to be used for manufacturing of drug substances, high pressures could lead to deactivation of the drug substance. Hence a pneumatic atomiser is preferred. Another aspect to consider is the liquid flowrates. The liquid flowrates used in the spray dryer are between 6- 35ml/min. Seeing these flowrates, a pneumatic atomiser is more effective to achieve atomisation. When it comes to droplet size, pneumatic atomisation is known to produce an overall smaller droplet size which is a requirement for inhaled medicines. Pneumatic atomisation is also more economical since it requires less energy input than hydraulic atomisation.

External Mixing

Since the nozzle is used to spray the drug product and the drug product can be sensitive to pressure, an external mixing nozzle is recommended. In an external mixing nozzle, the liquid pressure can be independent of the gas pressure whereas, in an internal mixing nozzle the liquid pressure has to be higher or equal to that of the atomising media (Hede, Bach, & Jensen, 2008). Internal mixing nozzles are however more efficient owing to the high energy transfer between the liquid and air streams. External mixing nozzles are less efficient but offer a high degree of control over droplet size since the gas and liquid flowrates can be manipulated independently of each other. Particle size is an important parameter to control while manufacturing inhaled medicines since it is the primary factor that determines the deposition and absorption of the medicines in lungs.

Spray Pattern

The nozzle has a full cone spray pattern. The only objective of the spray is to atomise the liquid and produce the required droplet size. The spray is placed inside a cylindrical drying chamber. Since a cone fits well inside a cylinder and due to the lack of special requirements which call for a different shape of the spray plume, a full cone spray pattern is beneficial since it maximizes the area of contact between droplets and drying air. The spray cone angle of the nozzle is based on the gas pressure. For the Schlick nozzle 970 S4 with a liquid orifice of 0.5, the spray cone angle varies between 30-40 degrees.

Swirling flow nozzle

The 970 S4 comes with angled grooves for the gas flow. This type of configuration imparts swirling action to the air and the air follows a spiral path. Swirling action helps separate the formed droplets by imparting centrifugal force to them. This motion aims to help in avoiding the droplets from coalescing and thus maintaining the achieved droplet size until the droplets are dried to form particles.

Objectives

The objectives set in this thesis are expected to contribute to the overall aim of better understanding the spray drying process for effective particle engineering via spray drying. Two main objectives are defined as follows and are aimed at gaining a better understanding of the atomisation process:

- To study the influence of composition on droplet size by varying surface active-excipient and Active Pharmaceutical Ingredient (API) and to correlate droplet size data with particle size data and physical properties.

- To establish a basis for futures studies on atomisation for use in Computational Fluid Dynamics (CFD) studies and droplet size prediction models.

Additionally, aspects related to characteristics of the nozzle, such as the effect of process parameters on droplet size and droplet breakup up models are identified at these process conditions. The effect of shear stress on the drug substance during atomisation is also touched upon.

Limitations

The study tests a limited number of formulations and does not offer the freedom to manipulate the composition of the formulations to achieve specific physical properties since in the bigger picture the composition has an important role to play in drug formulation and some constraints are to be met. The testing facility has limitations on the maximum gas and liquid flowrates that can be achieved during the experiments and hence only limited conditions are tested.

2. Theory

Atomisation is the process of creating fine droplets from a stream of liquid. Therefore, from a particle engineering perspective understanding droplet breakup is crucial to identify parameters that can be used to control and influence droplet size. From literature, it was found that spray formation and atomisation is still not a well understood phenomena. While various mechanisms are proposed and studied, most are limited in nature and work best only for the studied nozzle or only in specific conditions. Research still lacks a model that fits a wide range of sprays and their underlying conditions which lead to atomisation and a difference in their resulting attributes. Studies by (Lefebvre & McDonell, 2017); (Pilch & Erdman, 1987); (G.M Faeth & Wu, 1995); (Marmottant & Villermaux, 2004); (Guildenbecher, López-Rivera, & Sojka, 2009); etc. form the basis of most of the modern studies found today. Recent articles also emphasize the fact that a consensus on the underlying droplet breakup mechanisms that lead to droplet breakup is not yet reached (Jackiw & Ashgriz, 2022).

Briefly, atomisation is found to be a two-step process consisting of primary and secondary breakup. Primary breakup is a result of shear induced surface instability of two coflowing streams with different velocities and secondary breakup is a result of aerodynamic destabilisation of a separated droplet in the coflowing air. These instabilities are what govern droplet breakup from the bulk and lead to subsequent fragmentation. Primary breakup results in the formation of a primary droplet and this droplet later depending on its size, shape and speed is acted upon by aerodynamic forces which further destabilize the primary droplet leading to fragmentation. A schematic of the atomisation process is shown in Figure 3. A more technical discussion on how fragmentation takes place at each step follows and is later put into perspective for the performed experiments and is then discussed based on the results of the experimental findings.

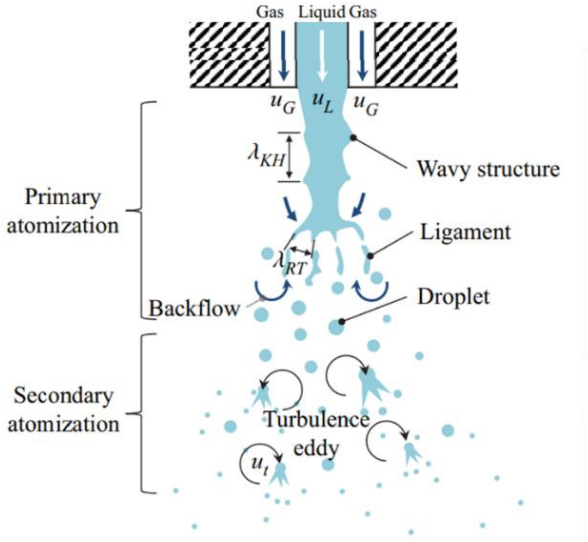

Figure 3: Schematic of the atomisation process (Choi, Byun, & Park, 2022) .

Shear induced surface instability

In pneumatic atomisation, two fluid streams i.e., gas and liquid flow corresponding to each other. The streams can be coflowing, crossflowing or turbulent. General behaviour of parallel coflowing streams is well explained by (Ling, Fuster, Tryggvason, & Zaleski, 2019). As the streams meet downstream, their velocity differences trigger a Kelvin-Helmholtz (KH) type of instability. Two initially parallel streams having different velocities are naturally unstable. As the streams meet downstream, their velocity differences trigger a Kelvin-Helmholtz type of instability. This is known as the Kelvin-Helmholtz

paradigm (Marmottant & Villermaux, 2004). The instability is induced by the difference in velocities between the parallel streams and the resulting shear between the gas-liquid interface near the nozzle (Ling, Fuster, Tryggvason, & Zaleski, 2019).

Kelvin-Helmholtz instability leads to the formation of waves at the interface with increasing amplitude. Formation of these instabilities can be seen in Figure 4(bottom left image for surface waves and bottom right image for growing amplitude and destabilising). Some studies conclude that the vorticity layer thickness of the gas stream at the inlet is the characteristic length scale that controls the selection of the most unstable wavelength in the induced instability (Ling, Fuster, Tryggvason, & Zaleski, 2019). Eventually, a point is reached in the growing wave amplitude where, the amplitude of the wave becomes comparable to the gas stream thickness. Thus, leading to a strong interaction between the interfacial wave and the gas stream. This causes the liquid sheet to pull from the crest and roll and to flap and break violently. Ling et al. (2019) also found that production of turbulent Kinetic energy was stronger in a gas-liquid mixing layer compared to a gas-gas mixing layer.

Marmottant & Villermaux (2004) give a comprehensive study of how a co-axial flow develops under the influence of increasing velocity of the coflowing destabilizing media such as air. The destabilization takes places in form of creation of ligaments at the air-liquid interface and can be seen in the images captured by (Marmottant & Villermaux, 2004) in Figure 4. Marmottant & Villermaux (2004) tested a variety of solutions with different physical properties and concluded that surface tension plays a crucial role in ligament spacing whereas differences in viscosity did not result in an appreciable difference in ligament spacing. These ligaments are then stretched under the influence of airflow. The rate of stretch and the thickness of ligaments at breakup depends strongly on air velocity (Marmottant & Villermaux, 2004). Ligament breakup occurs as a result of stretching and a decrease in ligament diameter leading to breakup (Marmottant & Villermaux, 2004).

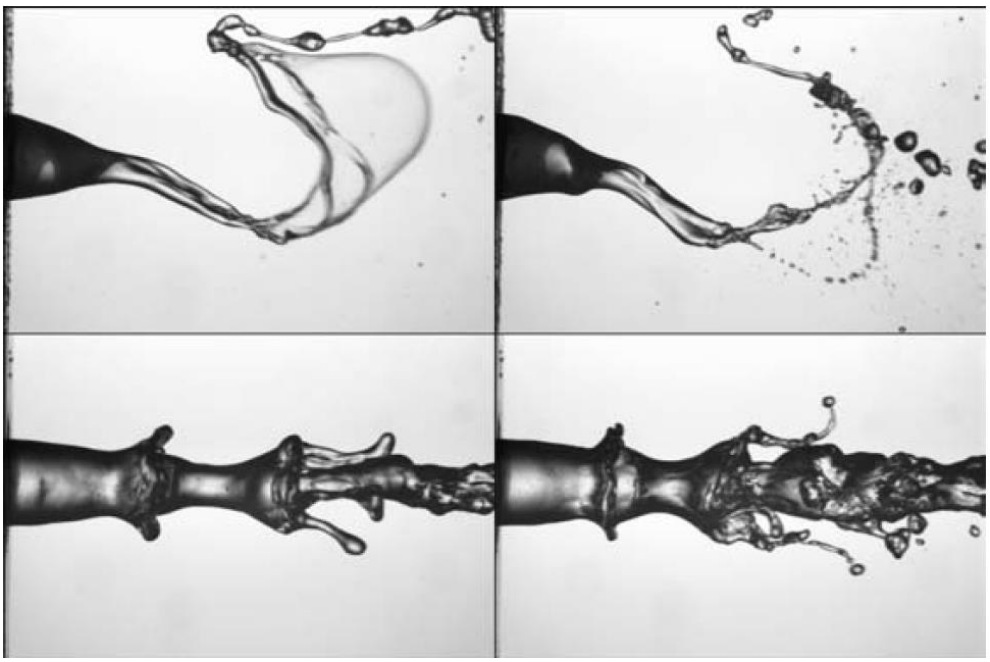

Figure 4: Development of instabilities imaged by (Marmottant & Villermaux, 2004). The top images are at low gas velocity and bottom images are at high gas velocity.

Studies on interfacial stability focus on downstream liquid breakup and the relation between upstream interfacial stability and downstream turbulence and spray characteristics have not been investigated thoroughly in literature (Ling, Fuster, Tryggvason, & Zaleski, 2019). Ling et al. (2019) state that the interfacial instability can be absolute or convective depending on the dynamic pressure ratios

or otherwise known as the Momentum Ratio (MR) between the two phases. The momentum ratio is defined as in equation (1).

$$M = \frac{\rho_g U_g^2}{\rho_l U_l^2} \quad (1)$$

For high momentum ratios, the instability is absolute (Ling, Fuster, Tryggvason, & Zaleski, 2019). When gas boundary layer is bigger than the separator region a transition from convective to absolute instability occurs. Huck et al. (2021) define a critical momentum ratio M_c = 50 above which the volume fraction profiles of the spray spread less than the gas phase. Fuster (2013) explain that a better understanding of the role of the splitter plate (the medium that separates the gas and liquid before they interact) is crucial to better predict wave growth and frequency, which in turn control the drop size and fluxes in applications related to atomization. Since ligaments form at different locations and possibly under vividly different conditions, their sizes are different, and the resulting droplets from ligament breakup are different in size from each other. The result is therefore a droplet size distribution from breakup of different ligaments.

Viscosity and surface tension are important characteristics that offer restoring forces to droplet breakup. Lower viscosity leads to smaller droplet size owing to the more elongated, thinner ligaments (Marmottant & Villermaux, 2004). The relevant dimensionless parameter identified for droplet breakup is Weber number. Above the critical Weber number, the droplet is considered to disintegrate. When the destabilizing flow is turbulent, the critical Weber number appears to be even lower (Marmottant & Villermaux, 2004). At higher Weber numbers, the droplet is stripped from its surface and a critical Weber number is not observed for this type of jet disintegration since the instability is capillarity driven (Marmottant & Villermaux, 2004). Transverse destabilization of the liquid stream is also possible in case of turbulent or swirling flow. Marmottant & Villermaux (2004) state that a balance between aerodynamic pressure and capillary pressure sets the size for the fragments that are peeled off. The ligament size is a function of the air speed and Reynolds number. The observed drop size corresponds to the primary corrugations formed. It starts with a Kelvin-Helmholtz instability and as the amplitude of modulations grow large enough, they undergo transverse destabilization of a Rayleigh-Taylor (RT) type (Marmottant & Villermaux, 2004).

Secondary aerodynamic destabilisation

Previously explained instabilities are responsible for production of primary droplets. These droplets are again subjected to aerodynamic forces in the influence of coflowing air. The droplets are then forced to deform and possibly break into fragments. Secondary breakup also referred to as secondary atomisation occurs further downstream. Fragmentation of these primary droplets continues until the aerodynamic drag has reduced the relative velocity between drops or fragments and the surrounding flow to a level where disruptive forces are no longer large enough to overcome restorative forces (Guildenbecher, López-Rivera, & Sojka, 2009). The time a droplet is subjected to disruptive forces should be sufficient to lead to breakup. Particulates and impurities can serve as initiation points for secondary breakup. Various breakup regimes and their mechanisms are summarised by (Guildenbecher, López-Rivera, & Sojka, 2009). Most mechanisms and their limits are set based on a low Ohnesorge numbers of <0.1 beyond which reliable research is not easily found. It is also thought that during the atomisation process in a spray, multiple breakup modes are at play simultaneously. Briefly, (Guildenbecher, López-Rivera, & Sojka, 2009) have defined five different regimes based on increasing Weber numbers. At lower Weber numbers between 0-11, breakup is considered as Vibrational breakup. Above 11 it then transitions to Bag type of breakup until 35. From 35-80 Multimode breakup is observed. Sheet-thinning type of breakup is observed between 80-350. Above a Weber number of 350 catastrophic breakup is observed. It is worth noting that these Weber number boundaries for transitions are approximate and, in their research, (Guildenbecher, López-Rivera, &

Sojka, 2009) found that different researchers defined different limits for transitions of breakup modes in their respective research. These mechanisms are illustrated in Figure 5 in the form of a schematic.

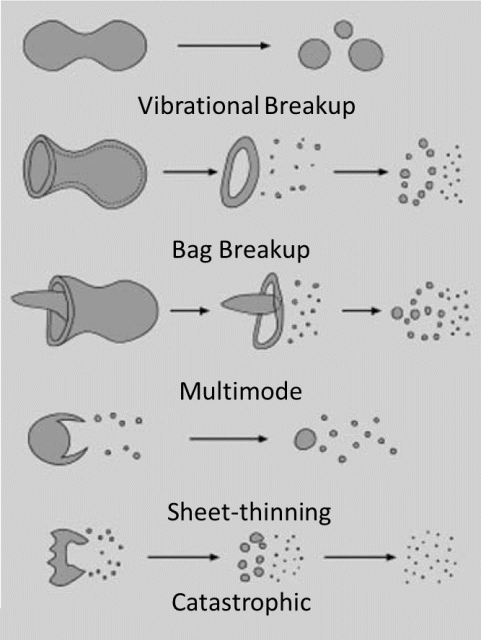

Figure 5: Secondary breakup mechanisms (Guildenbecher, López-Rivera, & Sojka, 2009) .

Another way to think about secondary breakup is that after primary breakup, the droplets formed have already been imparted with some velocity thus reducing the overall velocity difference and leading to different breakup mechanisms from that of primary breakup as seen in the top images from Figure 4 corresponding to low velocity breakup (bag breakup like mechanism can be observed).

More recent research on secondary atomisation mainly focusses on modified versions of the Taylor Analogy Breakup (TAB). In this model a droplet is said to oscillate similar to a mass-spring damper. Where viscosity is the damping force, aerodynamic force is the external force on the droplet and surface tension is the restoring force (Stefanitsis, Strotos, Nikolopoulos, Kakaras, & Gavaises, 2019). CFD modelling of droplet breakup is based on modified versions of the TAB model have noted to show good agreement with experimental data for vibrational and bag breakup regimes in their work and Modified Navier Stokes (M-NS) models show good agreement of the multimode and sheet-thinning breakup regimes. Stefanitsis et al. (2019) finally propose a unified model by combining the TAB and M-NS models.

A phase-space diagram can be used to find the spray regime and determine shape of the radial drop profiles of the spray. An illustration of the phase-space diagram from (Huck, Osuna-Orozco, Machicoane, & Aliseda, 2021) is seen in Figure 6. The different legends found in Figure 6 correspond to experimental findings from the works of different authors. In the phase-space diagram spray regime is identified using the Reynolds number of the liquid (Re_l) and the Weber number (We). The diagram is divided into 5 regimes. Regime I corresponds to 'U'- shaped profiles of the spray where flapping is dominant and larger droplets are seen towards the centre of the spray. Regime II corresponds to flat profiles of the spray which is observed with a reduction in the flapping stability due to increase in gas momentum. Regime III, IV and V correspond to '∩' shaped profiles with bigger droplets towards the edges of the spray. Regimes III and IV do not exhibit flapping due to recirculating gas cavities (Huck, Osuna-Orozco, Machicoane, & Aliseda, 2021).

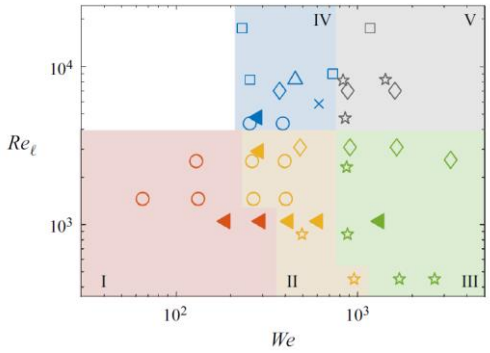

Figure 6: Phase-space diagram from (Huck, Osuna-Orozco, Machicoane, & Aliseda, 2021).

From the studied literature, transition between breakup regimes is found to be a function of Weber and Ohnesorge numbers and hence these were also used to characterise the studied nozzle and determine the regime of the spray. These dimensionless numbers are defined below.

Weber number

The Weber number is best defined by (Guildenbecher, López-Rivera, & Sojka, 2009) as the ratio of disrupting aerodynamic forces to restoring surface tension forces. Numerically written as in equation (2) where ρ is the density, v is the velocity, l is the characteristic length and σ is the surface tension.

$$We = \frac{\rho v^2 l}{\sigma} \tag{2}$$

The Weber number can be defined separately for primary and secondary atomisation. This is mainly due to the difference in the characteristic lengths at play. For primary atomisation, the Weber number is calculated using the gas shear-layer thickness δ as the characteristic length. δ is also widely accepted across literature as the characteristic length for primary breakup (Marmottant & Villermaux, 2004). The initial droplet diameter from primary breakup is used as the characteristic length for secondary atomisation (Guildenbecher, López-Rivera, & Sojka, 2009). Various other definitions of the characteristic length can be also be found for the calculation of Weber number in literature. Huck et al. (2021) have calculated the Weber number based on exit velocities and liquid and gas orifice diameters as the characteristic lengths. Watcher et al. (2020) use liquid jet diameter as characteristic length for calculation of Weber number.

Ohnesorge number

The Ohnesorge number is defined as the ratio of viscous forces to surface tension forces. The Ohnesorge number is expressed numerically in equation (3) where μ_d is the viscosity of the droplet and ρ_d is the density of the droplet.

$$Oh = \frac{\mu_d}{\sqrt{\rho_d d_0 \sigma}} \tag{3}$$

Since the Ohnesorge number deals typically with secondary breakup most researchers calculated it based on initial droplet diameter as the characteristic length. A higher Ohnesorge number indicates a lower tendency towards fragmentation due to internal viscous stabilization (Guildenbecher, López-Rivera, & Sojka, 2009).

Lastly, (Omidvar, 2019) modifies the (Pilch & Erdman, 1987) model and proposes the use of effective surface tension to combine turbulent effects with aerodynamic effects for secondary atomisation. The

effective surface tension is calculated based on the surface tension, drag induced stresses and turbulent induced stresses. It is claimed that the model shows good agreement with experimental and predicted data for droplet size and works with a Euler-Lagrange framework for CFD simulations. Poozesh et al. (2020) suggest velocity and droplet size prediction models based on conservation equations that correlate process conditions, formulation physiochemical parameters to droplet size distribution and velocity.

Overall, from the studied literature it is clear that the atomisation process is mix of various droplet breakup mechanisms acting at different positions in the spray as discussed and therefore leads to the formation of a droplet size distribution. It is also important to understand that a clear boundary between primary and secondary atomisation is not made and droplet breakup depends largely on the flow conditions and can lead to overlapping of these breakup mechanisms.

Effects of shear stress

Overall, based on the studied theory it is found that shear acts on the liquid at various locations in the spray and as a result can lead to destabilization of the protein structure (drug substance). Firstly, during primary breakup and secondly during secondary breakup. Bekard et al. (2011) in their review suggest that initial destabilization of the protein occurs at the solvent air interface or solvent solid interface where surface tension forces unfold the native protein. Atomization is a process where multiple air-liquid interfaces are formed during the process and hence it is possible that the drug substance is affected during this process. Bekard et al. (2011) also state that interfacial surface tension forces between air-water are estimated to be 140pN which is comparable to a protein denaturing force of 150pN. Bekard et al. (2011) finally highlight 3 criteria for shear stability of the protein molecule: the primary structure and molecular weight, the magnitude of shear strain and duration of its application and lastly, the viscosity of its surrounding medium. In another study by (Morgan, et al., 2020) the effect of shear stress on protein during the atomization process for spray drying was examined. Their research however concluded that the activity loss of protein due to shear is much higher in the spray drying process as compared to the atomization process. Based on the method used by (Morgan, et al., 2020), shear is calculated on the inside of the tip of the atomization nozzle. However, in the current study it is seen that shear continues to act at locations beyond the tip of the nozzle during the atomization process and is sustained for a period until the droplets have undergone substantial breakup. This has not been studied. Hence, more research is required to understand how shear can affect the active protein during the spray drying process.

3. Experimental set-up

This section expands on the measuring instrument used and explains how the equipment was setup for droplet size measurements and analysis of the spray. The section is divided into 3 parts: Droplet size measurement set-up, High speed imaging set-up and Measurement of physical properties.

Droplet size measurement set-up

For droplet size measurements, a Malvern Spraytec manufactured by Malvern Panalytical, UK was used. The atomising air was supplied by custom made pressure and flow control equipment present on site. Liquid was supplied using a peristaltic pump.

Malvern Spraytec

Malvern Spraytec is a state-of-the-art size distribution measurement instrument for aerosols and sprays. The instrument is capable of measuring at a speed of 10000Hz and covers a size distribution range of 0.1 to 2000 microns. It comes in two configurations, with either a 300mm or a 750mm lens. The 300mm lens configuration is used. The 300mm lens is capable of measuring a size distribution of the range 0.1µm to 900µm. Size distribution measurements done by the Spraytec are based on Light scattering. The instrument uses Mie theory and Fraunhofer approximation to estimate size distribution. The 300mm lens uses Mie theory for scattering of light. The instrument comes equipped with a 4mW He-Ne laser with a wavelength of 632.8nm as the light source. This light source is incident on the spray and the scattering signal is then detected by the detectors. The detection system has a total of 36 detectors to measure scattering signal. Three modes of measurement are possible: rapid, continuous and timed. Each mode of measurement gives information about a specific condition of a spray. The Spraytec offers reliable and reproducible results and is well tested in the industry.

Positioning of the nozzle

Two orientations of the nozzle were possible. The nozzle could be placed horizontally or vertically. In the spray dryer, conventionally, the nozzle is placed vertically. It was of interest to measure the spray vertically as is in the spray dryer. However, due to the construction of the of the Malvern Spraytec and the presence of active drug substance in formulations, vertical measurements were more difficult than anticipated. It was then decided to measure with the nozzle placed horizontally. To evaluate if there were significant differences in measuring horizontally versus vertically, droplet size of water was measured by placing the nozzle in both orientations while keeping the same distance between the nozzle tip and the centre of the laser beam. After the measurements, it was concluded that no significant difference was found with respect to the orientation of the nozzle. For all measurements, the nozzle was then placed horizontally in the same plane as the laser beam such that, centre of the spray plume would always align with the centre of the laser beam. Care was taken to consistently maintain the position of the nozzle until all the measurements were complete to ensure measurements were made at the same position in the spray for every formulation.

An important criterion for droplet size measurement was to find a point in the spray plume where the spray was well developed, and droplet coalescence or aggregation was minimal. It was chosen to keep a distance of 70mm from the tip of the nozzle to the centre of the laser beam and a distance of 70mm from the tip of the nozzle to the detector. The distance between the tip of the nozzle and detector was increased to later increased to 90mm since deposition of droplets on the detector was observed at higher gas flowrates. Thybo et al. (2008) and Watcher et al. (2020) also used similar distances for droplet size measurements using a similar atomiser thus indicating that the spray was fully developed beyond these distances.

Defining the measuring method for Malvern Spraytec

The measurement mode was set to timed measurements. The time for measurement was set to 30 seconds with one measurement done every 1 second resulting in a total of 30 measurements per spray setting. A time of 30 seconds was chosen since the spray was considerably stable and showed little

variation. The expected droplet size was below 100µm. The chosen lens of 300mm was capable of measuring droplets between 0.1µm to 900µm. The chosen lens was based on Mie-Scattering theory and since estimations using the Mie-scattering are based on refractive index, the refractive index of the solutions is calculated.

For calculation of refractive index an in-house software was used. The crystal structure was exported into the software along with its molecular weight. The software then gives the user a range of refractive indices with respect to molecular weight and wavelength. Of these values, the ones corresponding to 632nm which was also the wavelength of the laser used by the Malvern Spraytec were chosen. The refractive indices of the solutions are given in Table 1 below and samples are defined in Table 2.

Table 1: Refractive Index of formulations.

Formulation	Refractive Index
Sample 1	1.330519
Sample 2	1.330571
Sample 3	1.330645
Sample 4	1.330519
Sample 5	1.330571
Water	1.33
Air	1.00

As seen from Table 1, the refractive index for all solutions is very close to that of water. This is because the solutions are very dilute in nature and are mostly comprised of the solvent, water. The refractive index of sample 4 and sample 5 containing the active substance was assumed to be the same as that of sample 1 and sample 2 respectively, since no data was available on the active substance. Since all solutions are dilute, and the refractive index is very close to that of water, this assumption would not create a significant problem when it comes to measurements. Also, the existing data can be manipulated using the Spraytec software if desired at a later stage if needed. The scattering data for each measurement remains unaltered and can be manipulated based on the parameters one defines in the measuring method for the Spraytec.

The next part of the measuring method was defining the number of detectors to be included in the analysis. All 36 detectors were used in the analysis. Before each measurement, a background measurement was made for a period of 10 seconds. Errors with respect to background measurements were resolved by cleaning the lens and retaking the background measurement. No unusual characteristics were observed during the background and the droplet size measurements therefore using all detectors for the analysis was reasonable. With respect to fitting the data three options were available; no fit, a Rosin-Rammler fit and a log-normal fit. A no fit was chosen due to the occurrence of a bimodal size distribution. Multiple scattering was turned on as a correcting measure for multiple light scattering. The Spraytec employs mathematical correction for multiple scattering data and cannot guarantee a result free of multiple scattering. However, multiple scattering function is found reliable for multimodal size distributions (Triballier, Dumouchel, & Cousin, 2003).

One could also input the dimensions of the spray in terms of spray angle and distances from the detectors and nozzle tip, but this was observed to not affect the measurements significantly for the used nozzle and therefore only the path length for the laser beam was input to keep things simple.

The main variables of interest for each spray were Dv10, Dv50 and Dv90. These variables were recorded from the overall Particle Size Distribution. Overall, the same mathematical treatment was used for all measurements to maintain consistency.

Formulations to be tested

The total solids content was the basis for comparison for all the formulations. In spray drying, the solvent from the droplet evaporates and what is left behind is essentially just the solids content. For all formulations, the total solid content was set at 40mg/ml. The formulations were made from the same batch of excipients to ensure consistency between formulations. The formulations were made as listed in Table 2. For all formulations, the excipients were dissolved in solvent using an ice-cold bath and stirred overnight for complete dissolution. A clear solution without any precipitation indicated that the excipients were completely dissolved. A total of 250ml of each solution was made for droplet size measurement, viscosity, and surface tension.

Table 2: List of Formulations.

Formulation	Excipient			Active	Solvent
	A	B	C	D	Water
Sample 1	10%	Present	-	-	60%
Sample 2	15%	Present	-	-	60%
Sample 3	10%	Present	Present	-	60%
Sample 4	10%	Present	-	Present	60%
Sample 5	15%	Present	-	Present	60%

Experimental Design

The experimental design was based on the parameters of the manufacturing scale spray dryer. The liquids flowrate was 6ml/min with an atomising gas flow of 9.5kg/hr for the lab scale dryer while the commercial scale dryer used a liquid flowrate of 35ml/min with a gas flowrate of 13kg/hr. Due to limitations of the peristaltic pumping system, a maximum stable flowrate that could be achieved was 30ml/min. Alternatively, a bigger peristaltic pump could be used but since the arms were more spread out it created a pulsating effect of the spray at lower flowrates thus leading to increased complications in the measurements. Hence the smaller pump was chosen. Similar limitations were present for the gas flow system. A maximum flowrate of 8.5Nm^3/hr could be achieved which corresponds to a gas flowrate of 10kg/hr. Therefore, the limits of the experimental design were set as mentioned in Table 3.

Table 3:Experimental variable limits.

Variable	Lower	Upper
Liquid Flowrate	5ml/min	30ml/min
Gas Flowrate	3kg/hr	10kg/hr

An initial experimental design matrix was created using MODDE (experimental design software). A trial batch was run using this experimental matrix for one of the samples. The results of the experimental design were however inconclusive due to a number of reasons. Firstly, an experimental design only tested extreme ends of the characteristic. The testing range was too large to accommodate and understand the overall characteristic of the nozzle. Secondly, extreme ends meant using low liquid flowrates with high gas flowrates and vice versa. The Spraytec instrument struggled to make measurements at these ends which led to a lot of inconsistencies in the results. At low liquid flowrates and high gas flowrates, it led to a low scattering signal below 5%. This level of scattering was insufficient for the instrument to make measurements. At high liquid flowrates and low gas flowrates, it was difficult to measure since droplets would then deposit on the detector lens resulting in erroneous measurement showing a droplet size increase with time. It was then concluded that design of experiments is more suitable for optimisation and for a much smaller range of process parameters

as seen in the study conducted by (Dennison, et al., 2016). To fix this problem, it was decided to measure at different air to liquid ratios defined as in equation (4).

$$ALR = \frac{Gas\ flowrate\ (\frac{kg}{hr})}{Liquid\ flowrate\ (\frac{kg}{hr})} \quad (4)$$

A reference droplet size was measured using water to create a basis for comparison. The ALR was varied from 1.66 to 33.33. Three liquid flowrates were chosen for measurements. Namely, 5, 15 and 30ml/min. The gas flowrate was varied between 3-10kg/hr with increments of 1 for each of the three liquids flowrates. Water based measurements were used to understand the overall trend of the nozzle. For formulations, limited solution was available and therefore intermediate values were picked to estimate the characteristic. More measurements were made for lower liquid flowrates. Finally, the same characteristic was plotted for each sample. The reduced design for each sample is shown in Table 4.

Table 4: Experimental Design.

Gas flowrate		3	5	7	8	9	10
Liquid flowrate	5ml/min	√	√	√	√	√	√
	ALR	10	16.66	23.33	26.66	30	33.33
	15ml/min	√	√	-	√	-	√
	ALR	3.33	5.55	-	8.88	-	11.11
	30ml/min	√	√	-	√	-	√
	ALR	1.66	2.77	-	4.44	-	5.55

Before starting with the experiments, the pump calibration was checked and the pressure rating along with the expected gas flowrates through the nozzle were verified to be in order as the given specifications by Dusen Schlick.

High speed imaging set-up

High speed imaging was used to qualitatively assess and understand the spray. It was also expected to use the image for velocity mapping of the droplets. For high-speed imaging, a Photron Fastcam Mini AX100 was used.

Photron Fastcam Mini AX100

The Photron Fastcam Mini AX100 is a high-performance speed camera. It comes equipped with a 1024x1024 CMOS sensor and can shoot images at 4000 fps at full frame. The AX100 comes with a PFV software which can be used for particle tracking and motion analysis. The AX100 was coupled with a Tokina ATX 11-20mm F2.8 lens which enabled sharp and clear imaging. The camera is capable of shooting at a maximum of 540000fps with a much lower resolution of 128x16 pixels. The set-up was paired with a 200-Watt LED lamp to illuminate the spray.

Two different approaches of high-speed imaging were used to capture images of the spray. In the first, incident light on the spray plume was reflected and captured using, maximum possible exposure time. In the second, the powerful light source was placed directly pointing at the camera lens and the exposure was adjusted such that a shadow of the droplets was captured. The first approach was used for understanding how the primary droplet would form and behave and the second approach was used for theoretical mapping of droplet formation with respect to literature and identification of instabilities in the spray.

Measurement of physical properties

Surface tension

Surface tension was measured using a Biolin Tensiometer 702. Since the sample contained particles that behaved like surfactants, a Wilhelmy plate is preferred over a Du Noüy for surface tension measurements. However, a Wilhelmy plate was unavailable and hence, a Du Noüy ring was used for the measurements. Since only a comparative assessment of difference in surface tension of these was to be made, even though the absolute values might steer away from the ones measured, it is assumed that they are off by the same gradient. The data for surface tension of samples can be found in Table 5. Based on the measured values, the surface tension of water is lower than that obtained in the literature. Attempts were made to re-calibrate the tensiometer and re-do the measurements but to no success. The measured value was always lower than that of the literature value. Two other solutions: Acetone and Ethanol, were also tested for which the value of Acetone is lower than the literature value while Ethanol is very close to the literature value. Overall, the measurements can be used for comparative evaluation of solutions.

Viscosity

An Anton Paar Rheometer model MCR 302 was used for viscosity measurements. The temperature was set to 20 degrees Celsius for all measurements. For each measurement, the sample was subjected to shear forces of up to 1000 rpm. Beyond these values the viscosity was overestimated due to turbulent effects. The viscosity plots for all samples are shown in Figure 7. The viscosity measurements for all samples are listed in Table 5.

Table 5: Physical properties of samples.

Formulation	Surface Tension (mN/m)	Viscosity (cP)
Sample 1	46.19	1.1126
Sample 2	43.39	1.1364
Sample 3	53.18	1.1185
Sample 4	50.14	1.2554
Sample 5	48.65	1.2055
Water	68.73	1.0057
Ethanol	21.48	-
Acetone	23.04	-

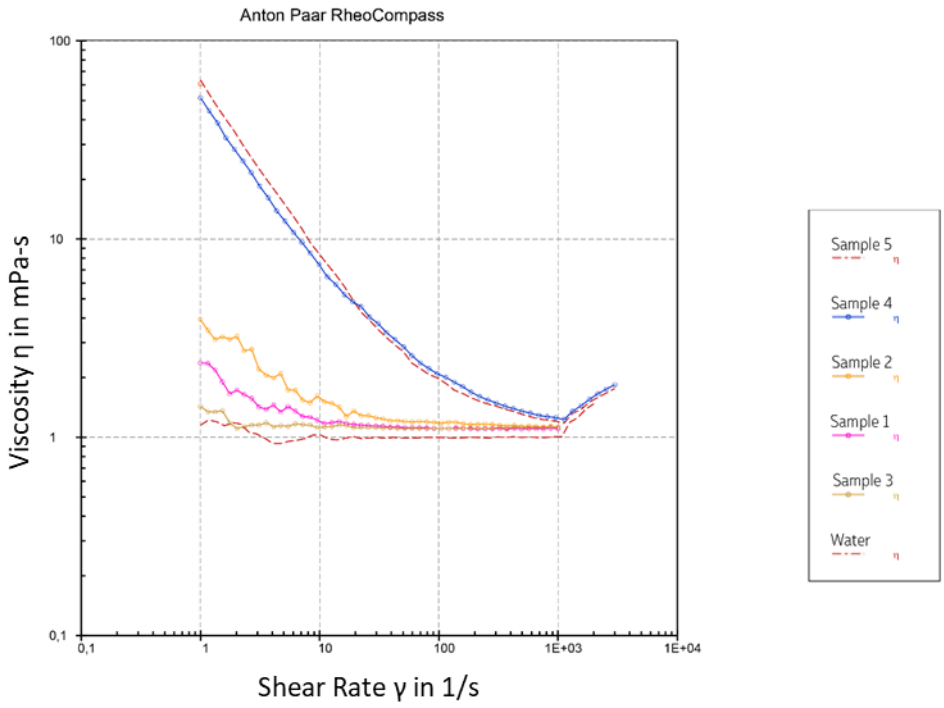

Figure 7: Viscosity measurement plots for samples.

Error of measurements

For calculating the absolute error, experiments were run after disassembling and reassembling the entire setup and on different days. Since each timed measurement consisted of 30 measurements in itself, the standard deviation was calculated by the Spraytec for every measurement sequence. The calculated standard error is given in Table 6.

Table 6: Calculation of standard error.

Exp	LFQ	GFQ	ALR	Dv50	SD	SE
1	30	6	3.333333	9.691	0.1332	0.006364
2	30	6	3.333333	9.709	0.1224	
3	30	8	4.444444	7.19	0.066	0.013435
4	30	8	4.444444	7.228	0.043	

4. Results and discussion

In this section the results from the experimental work are stated and following, the author's assessments regarding the results are discussed.

Influence of composition on droplet size

The droplet size data was plotted along with flow parameters to understand the characteristics of the nozzle. Trendlines for comparison of parameters including liquid flowrate, gas flowrate and ALR were plotted with respect to the droplet size. It was observed that the Dv50 varied linearly with respect to liquid flowrate. These characteristics are commonly found in literature. Reasons regarding the choice of Dv50 as the primary variable for comparison can be found in Appendix A. Dv50 varied with a power law characteristic when plotted against the gas flowrate and ALR. Gas flow is the main parameter affecting and governing the droplet breakup as will be seen in further discussions. It was also observed that plotting the Dv50 against ALR gives the best resolution for the graphs with fewer curves intersecting each other thus giving a clearer picture for comparison. The power law trend is also observed consistently in literature (Thybo, Hovgaard, Andersen, & Lindeløv, 2008); (Hede, Bach, & Jensen, 2008). A plot of the trend can be observed in Figure 8 for all tested formulations.

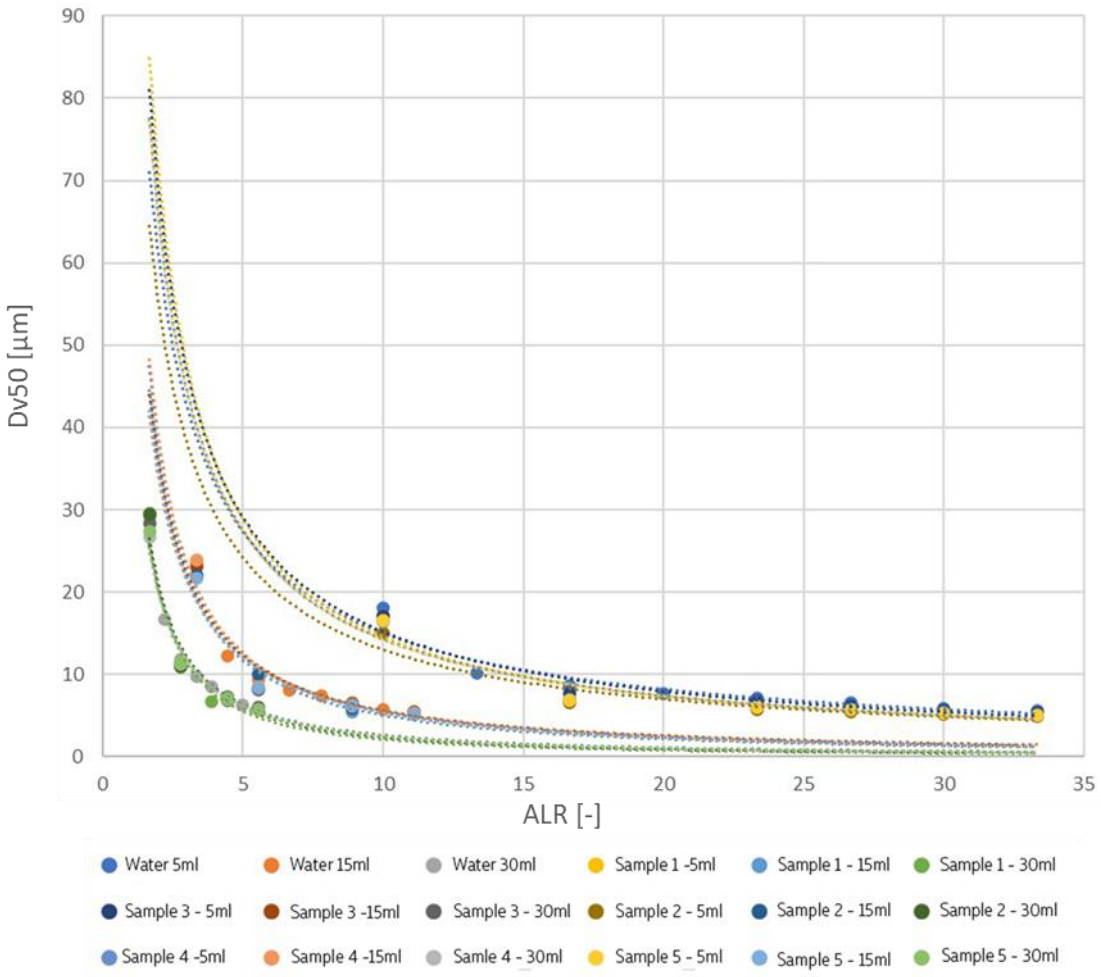

Figure 8: Graph of Dv50 vs ALR with trendlines.

The power law trend fits for all formulations tested irrespective of their viscosity and surface tension. Based on the trends in Figure 8 it can be said that initially with a small increase in gas flowrate a significant change in the droplet size can be observed. Eventually however a much higher change in

gas flowrates is required for a small change in the droplet size. The graph finally stabilizes for much higher ALRs indicating that the increasing the gas flow no longer has any influence on the droplet size. This indicates that at higher gas flowrates and small droplet diameters, the destabilizing stresses created during atomization can no longer overcome internal stabilizing stress. Also, an important factor to consider is that at this point (high gas flow and small droplet size downstream of the spray) in the atomization process the velocity gradient should have reduced significantly thereby reducing the effects of aerodynamic destabilization forces as the droplet now has lower inertia owing to its lower mass.

From Figure 8 it is observed that trendlines are found in three overlapping sets of lines. These sets correspond to the liquid flowrates. The outermost set corresponds to the lowest liquid flowrate of 5ml/min. The innermost corresponds to the highest liquid flowrate of 30ml/min. However spotting differences in droplet size for each of the compositions tested is quite difficult based on the graph in Figure 8 and it was used only to draw general conclusions pertaining to atomization characteristics of the formulations. Another thing to note from Figure 8 is that as the liquid flowrate increases, for the same gas flowrates the graph shifts towards the origin when plotted at the same ALR values. (Thybo, Hovgaard, Andersen, & Lindeløv, 2008) observed the same trend in their experiments. This implies that when investigating higher liquid flowrates there is lesser room for controlling the droplet size by varying the gas flow and settles for a much lower ALR. In a sense, the spray becomes more robust and less variable. These findings are considered valuable when considering equipment scaleup.

To assess the influence of changes in composition on droplet size, the droplet size data for each liquid flowrate was studied in isolation and the results are discussed based on observations made. Based on the results from the measurements seen in Figure 9 for a liquid flowrate of 5ml/min, it is observed that water has the highest overall droplet size at all given conditions of the spray. When comparing the differences in droplet size for the formulations, in terms of Dv50, the difference seems miniscule which makes it difficult to understand the changes. Hence, a different approach was used.

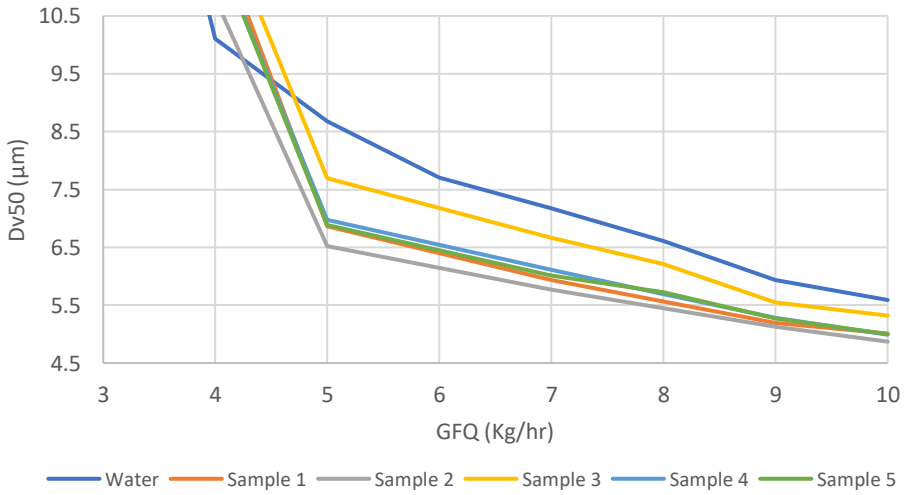

Figure 9: Dv50 vs GFQ for LFQ of 5ml/min.

A good way to compare the differences in droplet size is to scale up the droplet diameter to volume and check the difference in percentage. This method is considered as a better approach since what ends up as the solid particle is the total solids content and the total solids content depends on the volume of the droplet rather than the drop diameter. The difference in volume also reflects a direct difference in total solids content. The underlying assumption of this estimation is that the droplet is considered spherical. Practically however, the droplet could deviate from the shape of a sphere. Though drying can lead to differently shaped particles, it is a reasonable assumption to make. The data

for difference in volume is found in Figure 10. Graphs seen in the figure indicate how much lower in percentage is the overall volume of the droplet when compared to water for the same flow parameters.

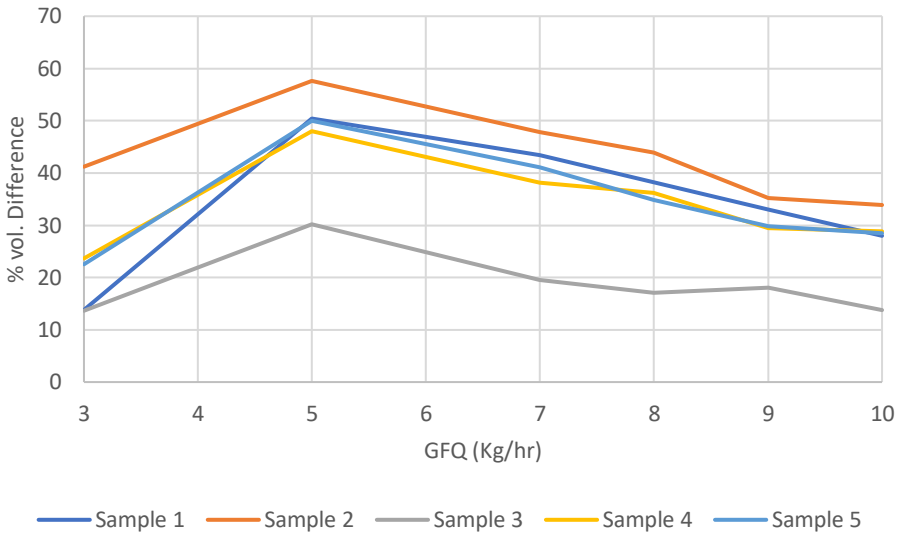

Figure 10: Percentage difference in volume compared to water droplet for LFQ of 5ml/min.

Comparing the graphs in Figure 10 based on concentration of excipient A, a trend follows. If higher amount of excipient A is present, the droplet size and hence the volume of the droplet is lower. Comparing sample 1 with sample 2 and comparing sample 4 with sample 5 it can be observed that 15% solutions have higher volume differences indicating lower total volumes. Presence of excipient C and active substance also affect the droplet size. Overall, based on the data we can observe that excipient A has a significant effect on droplet size. It is also worth noting that this trend was less clear at higher flowrates but overall showed lower droplet volumes than water.

Correlating droplet and particle size

The droplet size data was correlated with Particle Size Data (PSD) in µm at various gas pressures ranging from 3-10kg/hr and showed a good correlation at every tested pressure. A sample of the PSD data can be seen in Appendix B. Table 7 gives an overview of the droplet size data and PSD for 5kg/hr of gas flowrate and 5ml/min of liquid flowrate. Dv50 values and Dv90 values particularly showed higher positive correlation of 0.84 and 0.93 respectively whereas Dv10 shows significantly lower correlation of 0.31. Lower Dv10 correlation could be due to the design of the cyclone separator. The design of the cyclone separator is optimized to separate a fraction of the flow and it is expected that the much finer dried droplets could be ejected from the top of the cyclone.

Table 7: Correlation of droplet size with PSD.

	Dv50-droplet	Dv50-PSD	Dv10-droplet	Dv10-PSD	Dv90-droplet	Dv90-PSD
Sample 1	6.87	1.29	2.74	0.518	13.47	2.67
Sample 2	6.52	1.29	2.66	0.546	12.52	2.63
Sample 3	7.7	1.58	2.86	0.287	15.48	3.61
Sample 4	6.98	1.52	2.5	0.415	13.95	3.16
Sample 5	6.89	1.37	3.3	0.576	12.52	2.73
Correlation	0.840363		0.315476		0.937867	

It is also interesting that on correlating the data at all gas pressures a strong positive correlation is observed. Since the data correlates well for all irrespective of the gas pressure it can be assumed that similar drying conditions the same drying mechanism follows. However, on correlating data at different liquid flowrates, a good correlation but lower absolute values are observed and the correlation values are found to be quite variable at higher flowrates. Overall correlation values for Dv50 at all flowrates can be seen in Table 8. From Table 8, it appears that for two experimental conditions the correlation is negative, this is thought to be a result of errors in measurements. This indicates that droplet is of importance when it comes to controlling particle size and can be used to influence overall particle size.

Table 8: Correlation values for Dv50 at all liquid flowrates.

Correlation	LFQ (ml/min)		
GFQ(Kg/hr)	5	15	30
3	0.438765	0.797772	-0.63028
5	0.840363	-0.40845	0.524057
8	0.831952	0.762146	0.762934
10	0.756116	0.915084	0.76219

Correlating data with physical properties

To further strengthen the above observations the droplet size data was correlated using the physical properties. Physical properties and underlying physical mechanisms are what govern droplet breakup and eventually droplet size. Surface tension and viscosity are two fundamental properties of liquids which offer resistance to deformation. Figure 11 shows the correlation between the Dv50 values at 5ml/min liquid flowrate and 5kg/hr of gas flowrate with surface tension and viscosity of the solutions. The observations with respect to both properties is discussed further.

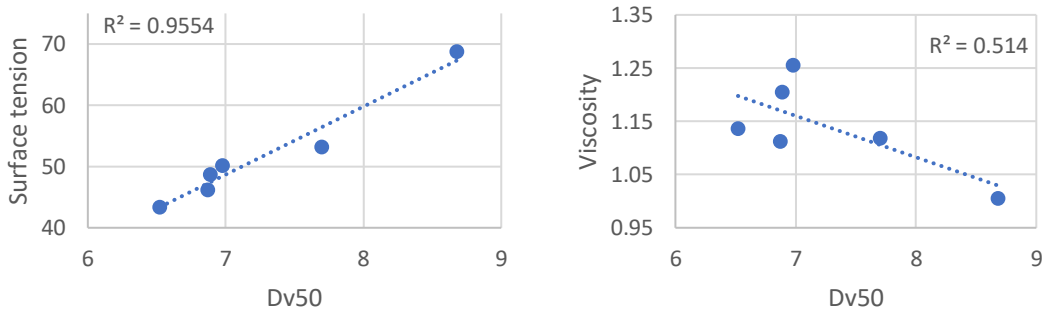

Figure 11: Correlation plots for surface tension and viscosity with Dv50.

Surface Tension

From Table 5 it is seen that water has the maximum surface tension of all the solutions. Sample 3 has the next highest surface tension of the formulations. When comparing these with the droplet size data it can be observed that water has the largest droplet size followed by sample 3. The smallest droplet size is that of the sample with the lowest surface tension which is sample 2. The surface tension for all formulations is lower than that of water and this data correlates well with the droplet size data. Overall, droplet size shows as strong positive correlation with surface tension with a R value of 0.97. Thus, indicating that the lower the surface tension the lower the droplet size owing to the lower restoring force.

Viscosity

The viscosity measurements however turned out very similar to each other as can be seen in Table 5. Based on the measured values it turns out that the added excipients have little to no effect on the solution in terms of the viscosity. They all are almost the same as that of water. Viscosity values were also correlated with Dv50 values. They show a good negative correlation with the droplet size data with a R value of -0.72. This indicates that having higher viscosity leads to smaller droplet size. It is worth mentioning that while all other solutions behaved Newtonian, the solutions with the active substance showed shear thinning characteristics as can be observed in Figure 7. Overall, owing to the little difference in viscosity values of the samples it is difficult to judge to what degree they affected the droplet size, but one can know that higher viscosity solutions will lead to smaller droplet size for the same atomizing conditions for low Ohnesorge numbers where surface tension forces dominate breakup. However, for high viscosity solutions, it is expected that viscosity of droplet will offer greater resistance to fragmentation thus impeding droplet breakup.

Characteristics of the nozzle and droplet breakup

Dimensionless numbers for the flow are calculated at all tested conditions to determine the characteristics of the nozzle and later droplet breakup is studied using high-speed imaging.

The momentum ratio is calculated for the studied gas and liquid flowrates using equation (1) and was found to be low for higher liquid flowrates and high for lower liquid flowrates. The calculated values can be found in the Momentum ratio part in the Appendix C. High momentum ratios are indicative of absolute instability as conveyed by (Ling, Fuster, Tryggvason, & Zaleski, 2019). An absolute instability is indicative of instability growth in the direction of the flow and is not convected laterally. The momentum ratio was found to be higher than the critical value of 50 for most flow conditions studied indicating that the spray spread is less than the gas spread. This explains why the spray cone angle of the nozzle is small at 40 degrees and is found to decrease further at higher gas flowrates. This is also indicative of why there was droplet deposition on the lens at 30ml/min and almost none at 5ml/min. It also indicates that bigger droplets are found towards the center of the spray and smaller droplets towards the edges of the spray and is observed in the high-speed images.

The Weber number is calculated using the formula given by (Huck, Osuna-Orozco, Machicoane, & Aliseda, 2021) based on the liquid and gas orifice diameters as the characteristic length. This method was chosen since the studied nozzles are very similar in function it was particularly easy to find and work with these values. The calculated values for the Weber number ranged between 1-20 (refer Appendix D) and the corresponding Reynolds number for liquid flow was below 1000. Based on the phase-space diagram by (Huck, Osuna-Orozco, Machicoane, & Aliseda, 2021) the spray nozzle tested falls under Regime I (refer Figure 6) for all experiments and can be matched with the U-shaped profiles as seen in the high-speed images. The U-shaped profile is where flapping of the liquid jet is dominant and can be seen in image sequence 10-15 in Appendix Figure C.

The Ohnesorge number was calculated for secondary breakup assuming that the primary droplet was between 0.5mm and 50µm in size and was found to be below 0.1 (refer Appendix E) for all flow conditions studied. This indicated that surface tension highly dominated secondary breakup as the restoring force.

Droplet breakup was studied with the help of sequential images from the high-speed camera and inspired by the work of (Xu, Wang, & Che, 2022) sequential images were mapped on to the velocity profile simulated in the work of (Vasudevan, 2020) for the same nozzle. The spray was imaged at the same conditions as in the CFD simulations and the images were used to analytically examine the spray. A good sequence of 25 images from the captured footage was identified and a few images emphasizing findings are shown in Figure 12. The entire sequence is found in the Appendix Figure C (refer Appendix F) and can be used to follow the entire breakup sequence from the formation and stretching of the RT instability to its disappearance. The gray part of each images is the tip of the nozzle with liquid insert

and orifice. The white part is the air cap. One image in the sequence roughly covers 8mm x 8mm space in reality. The images in Figure 12 were captured at 100,000 fps using very low exposure such that only the shadow of the image was seen in the image. The air pressure was set to 2.6 barg and liquid flowrate to 30ml/min. A second sequence at higher fps and lower liquid flowrates can be found in the Appendix Figure D (refer Appendix G).

As explained in the Theory section, Droplet breakup is a consequence of destabilizing stresses acting on the liquid stream. Formation and stretching of ligaments can be seen as a result of the Kelvin-Helmholtz instability near the nozzle tip. The liquid jet is seen to be stripped on the edges forming ligaments that are stretched and eventually break to form droplets. In Figure 12-image 14 it can also be seen that due to high velocity gradient, the ligaments curl and recirculate before breaking.

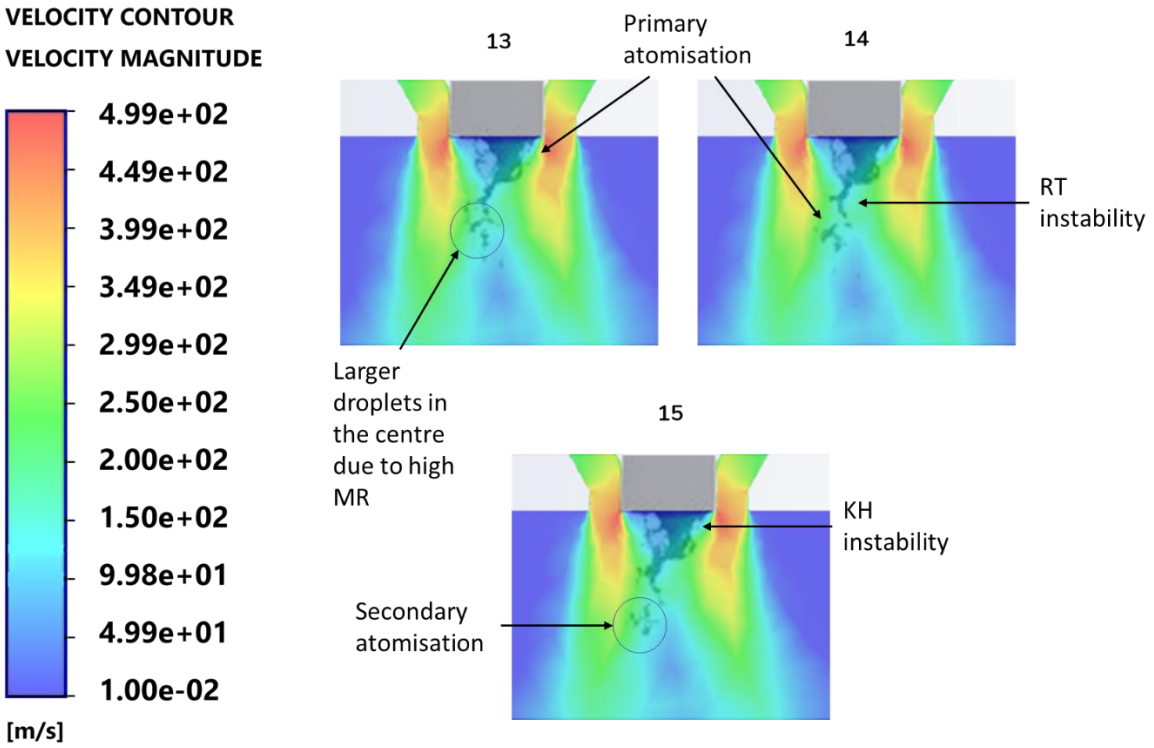

Figure 12: Isolated sequences (image13-15) from high-speed images superimposed on the velocity profiles showing various characteristics of the spray.

Transverse destabilization is seen in Figure 12-image 14 as a result of large amplitude modulations resulting in a Rayleigh-Taylor. Transverse destabilization is due to the low-density medium-air pushing the high-density medium-liquid which causes flapping of the liquid jet and is characteristic of Rayleigh-Taylor instabilities. These transverse destabilizations are a result of the swirling flow created by the nozzles. The above-mentioned mechanisms lead to primary breakup of the liquid stream. Secondary breakup however was significantly more difficult to capture given the low resolution of the images and the overall size of the primary droplets being very small. One can only see faint glimpses of secondary breakup on comparing Figure 12-images 14 and 15. The primary droplet is seen moving towards the higher gas flow before quickly disappearing due to drag generated by the gas flow.

As observed from the high-speed images, it is confirmed that primary breakup is from a mix of Rayleigh-Taylor and Kelvin- Helmholtz instabilities since both mechanisms can be observed in the high-speed images. At lower flowrates however it appears that Rayleigh-Taylor instabilities dominate and can be seen in the image sequence in the Appendix Figure D. It is also possible that at lower flowrates the spray was not dense enough to capture Kelvin-Helmholtz instabilities well enough with the camera setting used.

Overall, droplet size has good positive correlation with surface tension. This is reasonable considering that fact that the primary restoring force for droplet formation is surface tension. A lower surface tension thus indicates lower restoring force, resulting in lower resistance to breakup and leading to the formation of a comparatively smaller droplet. Viscosity has good negative correlation with droplet size indicating higher viscosity leads to smaller droplet size. This can be explained based on the fact that higher viscosity leads to formation of longer ligaments as they can be stretched further than lower viscosity solutions before, they breakup. Longer ligaments are thinner and thus lead to smaller droplets upon breakup. Thereby verifying and justifying the experimental observations with theoretical mechanisms.

5. Conclusion

In this thesis, the influence of change in composition on droplet size was studied by varying surface-active excipient and API and a difference in droplet size was observed for all formulations. Higher the amount of surface-active excipient, smaller the droplet size. Droplet size data was further correlated with particles size data and a good correlation was obtained for the Dv50 and Dv90 data. The data was also correlated with physical properties of the solutions, surface tension and viscosity. It was found that surface tension and viscosity both correlated well with the droplet size data. A lower surface tension indicated smaller droplet size and a lower viscosity indicated larger droplet size. These correlations were then justified using mechanisms found in the theory. Therefore, to facilitate particle engineering, the droplet size can also be modified by manipulating the surface tension and viscosity of solutions since they are the restoring forces that resist breakup.

A Schlick 970 S4 nozzle with a 0.5mm liquid insert and underlying droplet breakup mechanisms were studied from literature and identified with the help of high-speed imaging. It is found that breakup takes place in two stages: primary and secondary breakup. Primary breakup is due to Kelvin-Helmholtz and Rayleigh-Taylor instabilities and secondary breakup is due to aerodynamic forces. The Momentum ratio, Weber number and Ohnesorge number were calculated for the flow conditions and breakup regime was identified according to literature. Primary breakup was found to be dominated by shear destabilisation and secondary by aerodynamic destabilisation.

The velocity of droplets could not be measured using the high-speed camera set-up given the low resolution of the images and the rapid changes in subsequent images. Current droplet size prediction models are ineffective to predict the small droplet size differences as observed in these studies. The two-step breakup process further complicates predictions models.

Overall, the work done in this project sets comparison criteria for formulations to control droplet size and in turn particle size for inhaled medicines. It also identifies some baselines for further studies on external mixing atomisation nozzles. The characteristics of the nozzle expressed in this work nozzle can be used to find suitable models for CFD studies in atomisation and droplet size prediction.

6. Future Scope

From a drug formulation and particle engineering perspective, it is recommended to assess how the individual excipients affect the properties of the solution. This will then help understand how concentration of individual excipients can be used to modify the droplet size and the resulting particle size. Secondly, a study of how these changes in these concentrations of excipients affect the characteristics of the dried particles must be conducted.

The work of (Poozesh, Akafuah, Campbell, Bashiri, & Saito, 2020) can be used as a reference to build velocity and droplet size prediction models. The proposed model by (Poozesh, Akafuah, Campbell, Bashiri, & Saito, 2020) is based on conservation equations and correlates process conditions, formulation physiochemical parameters to droplet size distribution and velocity. Alternatively, the analytical model suggested by (Omidvar, 2019) can also be tested to predict the Sauter Mean Diameter since it is claimed to work with Euler-Lagrange framework. If this model is found to work well, it could also be used for the estimation of stresses acting on the fluid during the atomisation process.

References

Alhajj, N., O'Reilly, N. J., & Cathcart, H. (2021). Designing enhanced spray dried particles for inhalation: A review of the impact of excipients and processing parameters on particle properties. *Powder Technology*, 313-331.

Basics of nozzle technology. (2022). Retrieved from www.lecher.com: https://www.lechler.com/de-en/technology/basics-nozzle-technology

Bekard, B. I., Asimakis, P., Bertolini, J., & Dunstan, E. D. (2011). The Effects of Shear Flow on Protein Structure and Function. *Biopolymers Volume 95/Number 11*, 733-745.

Boel, E., Koekoekx, R., Dedroog, S., Babkin, I., Vetrano, M. R., Clasen, C., & Mooter, G. V. (2020). Unraveling Particle Formation: From Single Droplet Drying to Spray Drying and Electrospraying. *Pharmaceutics12(7)*, 625.

Choi, D., Byun, J., & Park, H. (2022). Analysis of liquid column atomisation by annular dual nozzle gas jet flow. *Journal of Fluid Mechanics 943*, A25.

Daniel Fuster, J.-P. M. (2013). Instability regimes in the primary breakup region of planar coflowing sheets. *Journal of Fluid Mechanics, 736*, 150-176.

Dennison, T. J., Smith, J., Hofmann, M. P., Bland, C. E., Badhan, R. K., Al-Khattawi, A., & Mohammed, A. R. (2016). Design of Experiments to Study the Impact of Process Parameters on Droplet Size and Development of Non-Invasive Imaging Techniques in Tablet Coating. *PLoS ONE 11(8): e0157267*.

Dusen-Schlick GmBH. (2022). *Model 970*. Retrieved from myschlick.com: https://www.myschlick.com/en/products/two-substance-nozzles/external-mixing/970

G.M Faeth, L.-P. H., & Wu, P.-K. (1995). Structure and breakup properties of sprays. *International Journal of Multiphase Flow, Volume 21*, 99-127.

Gil-Chávez, J., Padhi, S. S., Hartge, U., Heinrich, S., & Smirnova, I. (2020). Optimization of the spray-drying process for developing aquasolv lignin particles using response surface methodology. *Advanced Powder Technology, Vol. 31, Issue 6*, 2438-2356.

Guildenbecher, D., López-Rivera, C., & Sojka, P. (2009). Secondary atomization. *Experiments in Fluids, 46*, 371-402.

Hede, P. D., Bach, P., & Jensen, A. D. (2008). Two-fluid spray atomisation and pneumatic nozzles for fluid bed coating/agglomeration purposes: A review. *Chemical Engineering Science, Vol. 63, Issue 14*, 3821-3842.

Huck, P., Osuna-Orozco, R., Machicoane, N., & Aliseda, A. (2021). Spray dispersion regimes following atomization in a turbulent co-axial gas jet. *Journal of Fluid Mechanics, 932*, A36.

Jackiw, I. M., & Ashgriz, N. (2022). Prediction of droplet size distribution in aerodynamic droplet breakup. *Journal of Fluid Mechanics, 940*, A17.

Lefebvre, A. H., & McDonell, V. G. (2017). *Atomisation and Sprays.* Boca Raton: CRC Press.

Ling, Y., Fuster, D., Tryggvason, G., & Zaleski, S. (2019). A two-phase mixing layer between parallel gas and liquid streams: multiphase turbulence statistics and influence of interfacial stability. *Journal of Fluid Mechanics, 859*, 268-307.

Malvern Instruments Limited. (2015). *A basic guide to particle characterisation.* Retrieved from cif.iastate.edu:https://www.cif.iastate.edu/sites/default/files/uploads/Other_Inst/Particle%20Size/Particle%20Characterization%20Guide.pdf

Marmottant, P., & Villermaux, E. (2004). On Spray Formation. *Journal of Fluid Mechanics, 498*, 73-111.

Matas, J.-P., & Cartellier, A. (2013). Flapping instability of a liquid jet. *Comptes Redus Mecanique, Vol. 341, Issue 1-2*, 35-43.

Morgan, B. A., Manser, M., Jeyanathan, M., Xing, Z., Cranston, E. D., & Thompson, M. R. (2020). Effect of Shear Stresses on Adenovirus Activity and Aggregation during Atomization to produce Thermally Stable Vaccines by Spray Drying. *ACS Biomaterials Science & Engineering, 6*, 4304-4313.

Omidvar, A. (2019). Development and assessment of an improved droplet breakup model for numerical simulation of spray in a turbulent flow field. *Applied Thermal Engineering, Vol. 156*, 432-443.

Pilch, M., & Erdman, C. A. (1987). Use of breakup time data and velocity history data to predict the maximum size of stable fragments for acceleration-induced breakup of a liquid drop. *International Journal of Multiphase Flow, Vol.13, Issue 6*, 741-757.

Poozesh, S., Akafuah, N. K., Campbell, H. R., Bashiri, F., & Saito, K. (2020). Experiemental and Mathematical Tools to Predict Droplet Size and Velocity Distribution for a Two-Fluid Nozzle. *Fluids, 5 (4)*, 231.

Reinhard, V. (2008). Pharamaceutical Particle Engineering via Spray Drying. *Pharmaceutical Research, Vol. 25*, 999-1022.

Stefanitsis, D., Strotos, G., Nikolopoulos, N., Kakaras, E., & Gavaises, M. (2019). Improved droplet breakup models for spray applications. *International Journal of Heat and Fluid Flow, Vol. 76*, 274-286.

Surendra, K. S., & Pankaj, S. K. (2021). Liquid jet breakup and spray formation with annular swirl air. *International Journal of Multiphase Flow, Vol.134*, 103474.

Thybo, P., Hovgaard, L., Andersen, S. K., & Lindeløv, J. S. (2008). Droplet Size Measurements for Spray Dryer Scale-Up. *Pharamaceutical Development and Technology, 13(2)*, 93-104.

Triballier, K., Dumouchel, C., & Cousin, J. (2003). A technical study on the Spraytec performances: influence of multiple light scattering and multi-modal drop-size distribution measurements. *Experiments in Fluids, 35*, 347-356.

Vasudevan, S. (2020). *Modeling of multiphase flows in a spray dryer.* Gothenburg: Chalmers University of Technology.

Watcher, S., Jakobs, T., & Kolb, T. (2020). Effect of Solid Particles on Droplet Size Applying the Time-Shift Method for Spray Investigation. *Applied Sciences, 10(21)*, 7615.

Xu, Z., Wang, T., & Che, Z. (2022). Droplet breakup in airflow with strong shear effect. *Journal of Fluid Mechanics, 954*, A54.

Appendix A

Droplet size measurements

In order to characterize the spray for each formulation, the droplet size distribution was looked at. A sample reading from the Malvern Spraytec is shown in Appendix Figure A. Primarily, values of Dv10, Dv50 and Dv90 were looked at. These values were selected since particle size data was available in terms of the same values and therefore it would be possible to correlate the two. From Appendix Figure A, the droplet size distribution appears to be an almost bimodal size distribution. This trend was observed for almost all the tested formulations. The first peak observed is made up of very fine droplets ranging from 0.5µm to 5µm. These fines are assumed to disappear when dried via the cyclone separator. Majority of the spray is made up of particles close to that of the Dv50 value. This can be observed in Appendix Figure A when looking at the tabulated data from the Malvern Spraytec. Maximum volume percentages are found close to the Dv50 values of the spray. Close to 40% of all the droplets exist at approximately this size in the spray. Hence it is safe to assume that this makes up the bulk of the spray. Therefore, Dv50 was set as the primary factor for comparison of the formulations.

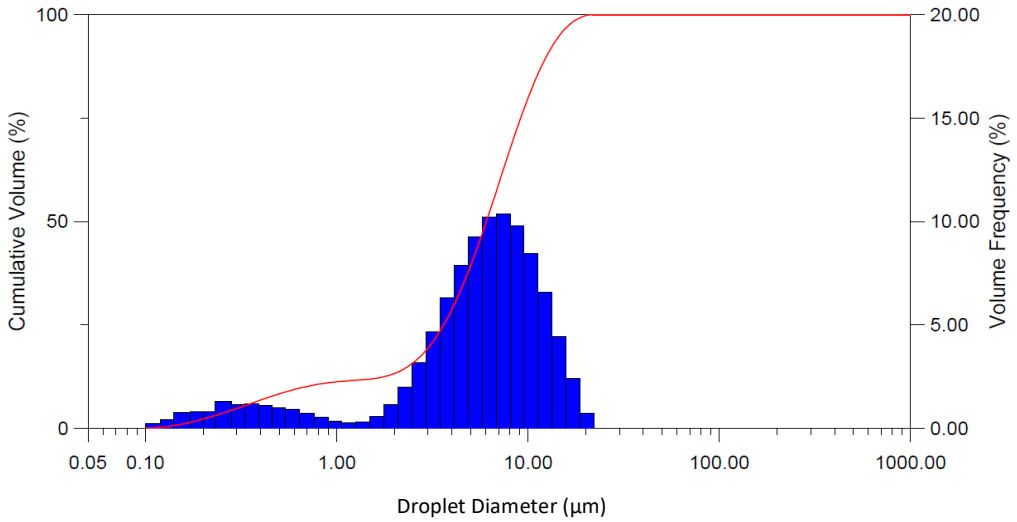

Droplet Diameter (µm)

Size (µm)	% V <	% V	Size (µm)	% V <	% V	Size (µm)	% V <	% V
0.120	0.25	0.25	3.46	23.51	4.68	101.22	100.00	0.00
0.140	0.67	0.42	4.10	29.84	6.33	119.83	100.00	0.00
0.170	1.43	0.76	4.85	37.71	7.87	141.86	100.00	0.00
0.200	2.26	0.83	5.74	46.96	9.25	167.94	100.00	0.00
0.230	3.08	0.82	6.80	57.16	10.20	198.82	100.00	0.00
0.280	4.37	1.29	8.05	67.53	10.37	235.37	100.00	0.00
0.330	5.52	1.15	9.53	77.32	9.80	278.65	100.00	0.00
0.390	6.70	1.18	11.28	85.79	8.47	329.88	100.00	0.00
0.460	7.82	1.13	13.36	92.39	6.60	390.53	100.00	0.00
0.540	8.83	1.01	15.81	96.84	4.45	462.33	100.00	0.00
0.640	9.76	0.93	18.72	99.27	2.43	547.33	100.00	0.00
0.760	10.50	0.75	22.16	100.00	0.73	647.96	100.00	0.00
0.900	11.03	0.53	26.23	100.00	0.00	767.09	100.00	0.00
1.06	11.38	0.34	31.06	100.00	0.00	908.13	100.00	0.00
1.26	11.64	0.26	36.77	100.00	0.00	1075.09	100.00	0.00
1.49	11.93	0.30	43.53	100.00	0.00	1272.75	100.00	0.00
1.76	12.50	0.56	51.53	100.00	0.00	1506.76	100.00	0.00
2.09	13.65	1.15	61.00	100.00	0.00	1783.79	100.00	0.00
2.47	15.65	2.00	72.22	100.00	0.00	2111.75	100.00	0.00
2.92	18.83	3.18	85.50	100.00	0.00	2500.00	100.00	0.00

Appendix Figure A: Sample of the droplet size distribution graphical output (above) and tabulated (below) by the Malvern Spraytec for the same spray conditions.

Appendix B

Particle size distribution

A sample of the Particle Size Distribution (PSD) is shown in Appendix Figure B below. The average of the two readings was used to correlate the data with droplet size data. The PSD data is generated for one set flowrates.

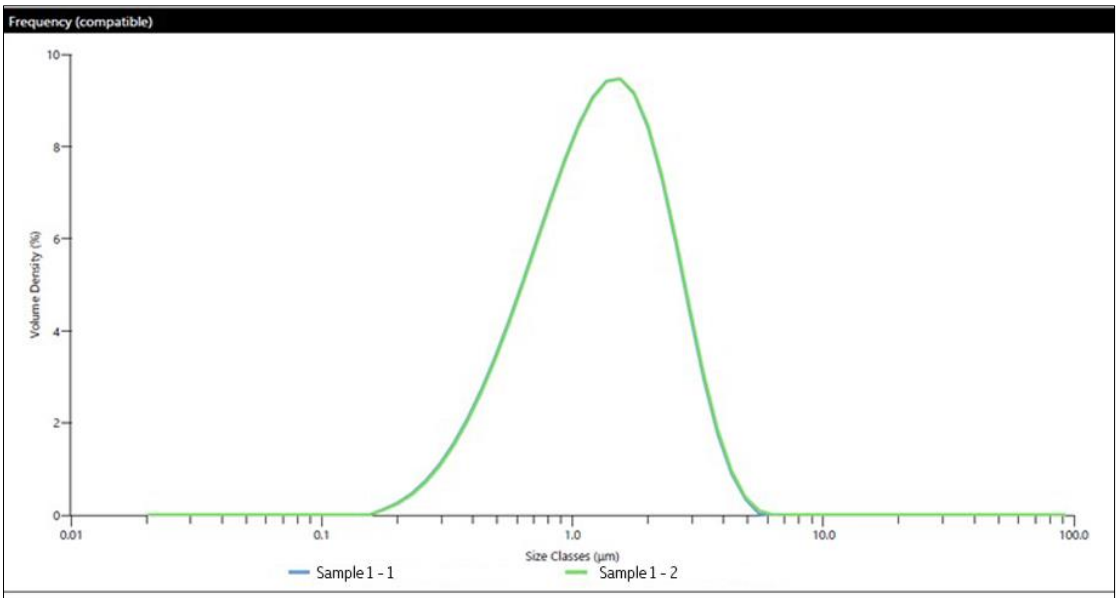

Trend

	Record Number	Sample Name	Dx (10) (µm)	Dx (50) (µm)	Dx (90) (µm)
	2	Sample 1 - 1	0.515	1.28	2.65
	3	Sample 1 - 2	0.522	1.29	2.68
Mean			**0.518**	**1.29**	**2.67**
1xStd Dev			**0.00486**	**0.00878**	**0.0206**
1xRSD (%)			**0.938**	**0.682**	**0.772**

Appendix Figure B: PSD for Sample 1.

Appendix C

Momentum ratio

The momentum ratio is calculated using equation (1). The ratio was calculated at the three different flowrates used in the experimental design. The calculated values are given in Appendix Table A.

Appendix Table A: Calculated Momentum Ratio.

Gas flowrate (Nm3/hr)	Liquid flowrate		
	5gm/min	15gm/min	30gm/min
2.575107	809.3873	89.93193	22.48298
3.433476	1438.911	159.879	39.96974
4.291845	2248.298	249.8109	62.45273
5.150215	3237.549	359.7277	89.93193
6.008584	4406.664	489.6294	122.4073
6.866953	5755.643	639.5159	159.879
7.725322	7284.486	809.3873	202.3468
8.583691	8993.193	999.2436	249.8109

Appendix D

Weber number

The Weber number was calculated using the formula by (Huck, Osuna-Orozco, Machicoane, & Aliseda, 2021).

$$We = \frac{\rho_g {U_g}^2 d_l}{\sigma}$$

Where d_l is the liquid orifice diameter. The above equation was selected since the type of the nozzle used by (Huck, Osuna-Orozco, Machicoane, & Aliseda, 2021) was very similar to one tested in this study. The calculated Weber numbers at various flow conditions are given in Appendix Table B.

Appendix Table B: Calculated Weber number for samples.

Gas flowrate (Nm3/hr)	Weber Number					
	Water	Sample 1	Sample 2	Sample 3	Sample 4	Sample 5
2.575107	1.099576	1.636153	1.741735	1.421096	1.507257	1.55342
3.433476	0.460999	2.908716	3.096418	2.526393	2.679569	2.761636
4.291845	0.720311	4.544868	4.838153	3.947489	4.186826	4.315056
5.150215	1.037248	6.54461	6.966941	5.684384	6.02903	6.21368
6.008584	1.41181	8.907942	9.48278	7.737079	8.206179	8.457509
6.866953	1.843996	11.63486	12.38567	10.10557	10.71828	11.04654
7.725322	2.333808	14.72537	15.67562	12.78986	13.56532	13.98078
8.583691	2.881244	18.17947	19.35261	15.78996	16.7473	17.26022

From Appendix Table B it can be seen that the Weber number varies between 1-20 for all flow conditions. This gives us the Weber number for primary atomisation. Since the Weber number for secondary breakup is directly proportional to the primary droplet diameter, it follows that the Weber number will be even lower since primary droplets formed are smaller.

Appendix E

Ohnesorge number

The Ohnesorge number is calculated using equation (3) based on formula given by (Guildenbecher, López-Rivera, & Sojka, 2009). The calculated Ohnesorge numbers are given in Appendix Table C and are calculated based on two assumed initial droplet diameters.

Appendix Table C: Calculated Ohnesorge number for samples.

d_o (mm)	Ohnesorge Number					
	Water	Sample 1	Sample 2	Sample 3	Sample 4	Sample 5
0.005	0.054333	0.073322	0.077269	0.068696	0.079407	0.077409
0.5	0.005433	0.007332	0.007727	0.00687	0.007941	0.007741

The Ohnesorge numbers in Appendix Table C are based on upper and lower estimates of the primary droplet. For Primary droplet diameters below 0.001mm, the Ohnesorge number is calculated to go above 0.1.

Appendix F

High speed image sequence 1

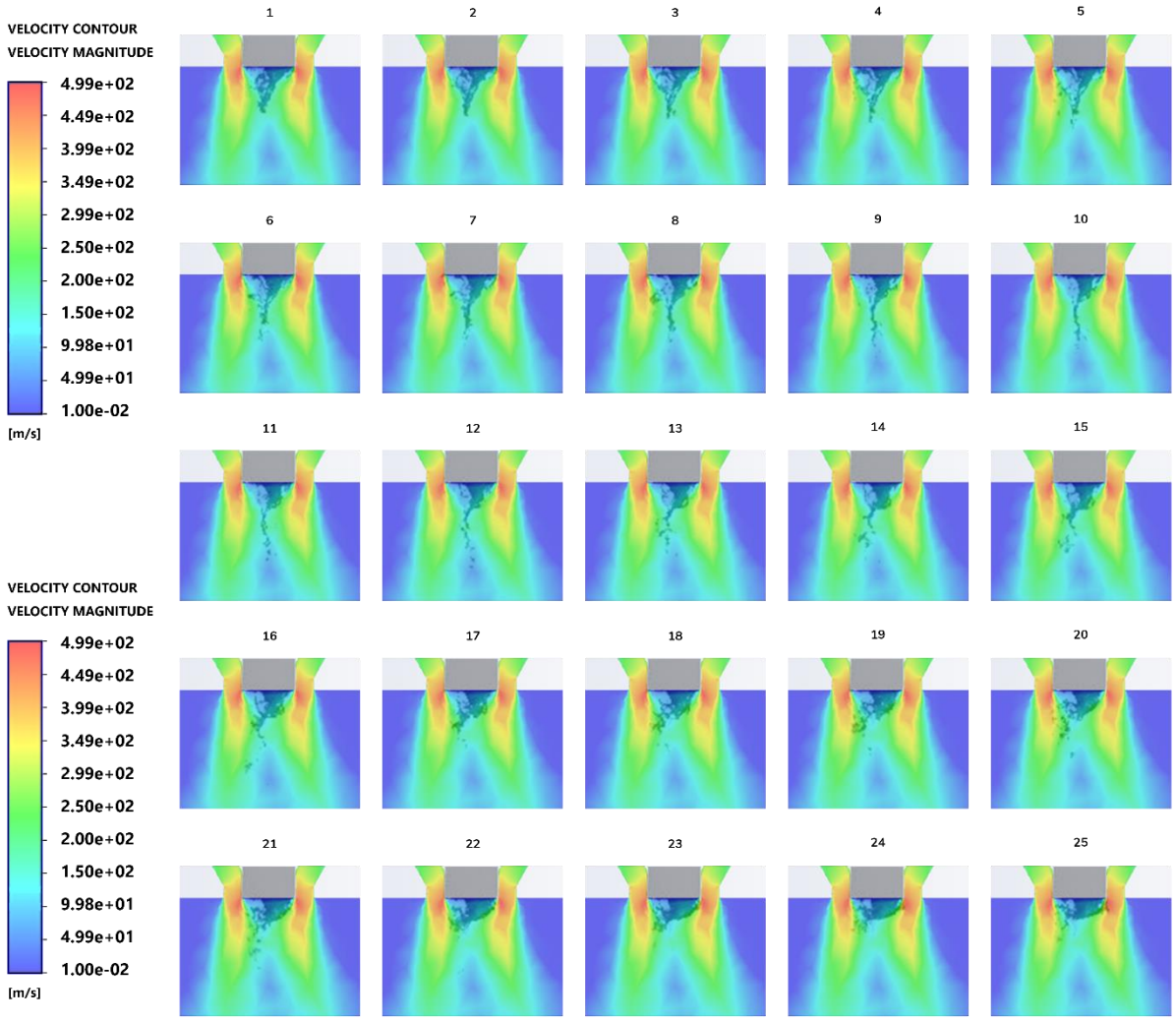

Appendix Figure C: High-speed image sequence 1 showing the formation of instabilities till breakup.

The above sequence in Appendix Figure C was imaged at 100,000 fps at a pressure of 2.6 bar and liquid flowrate of 30ml/min. This sequence of images shows the formation surface waves due to KH instability and also the formation and stretching of ligaments due to the RT instability.

Appendix G

High speed image sequence 2

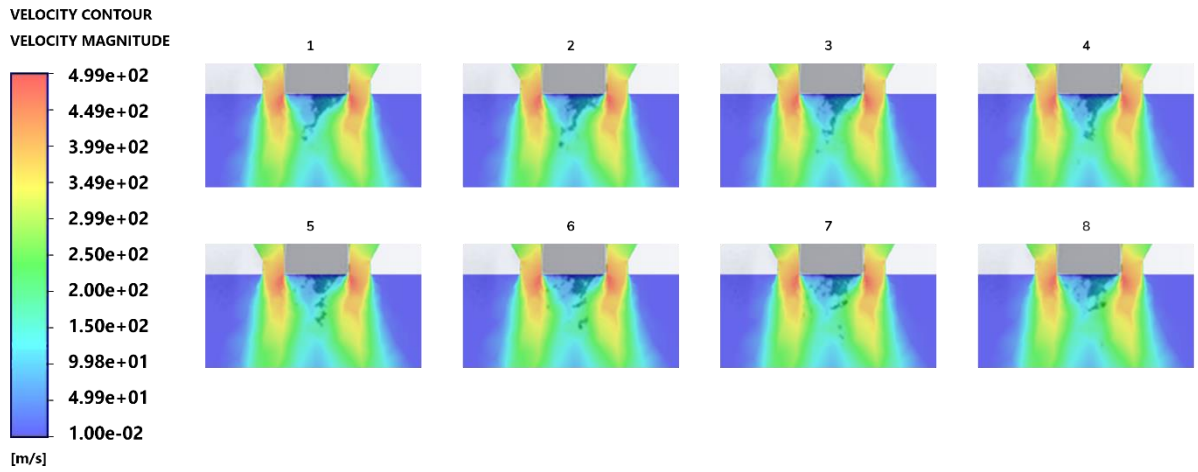

Appendix Figure D: High-speed image sequence 2(lower liquid flowrate & higher FPS).

The above sequence in Appendix Figure D was imaged at 127,000 fps at a pressure of 2.6 bar and liquid flowrate of 5ml/min. In the above sequence, formation of a Rayleigh-Taylor instability is seen in starting to develop in image 3 eventually curving inwards in image 4 and finally breaking off on image 5. Image 6 and 7 show secondary breakup in progress.

DEPARTMENT OF CHEMISTRY AND CHEMICAL ENGINEERING
CHALMERS UNIVERSITY OF TECHNOLOGY
Gothenburg, Sweden 2022
www.chalmers.se

CHALMERS
UNIVERSITY OF TECHNOLOGY